Biopsy Needle Puncture Path Planning Method based on 3D Ultrasound Images

Yue Zhao[1, 2], *IEEE member*, Hongyu Qi [1, 3], Dandan Li [1, 2], *IEEE member*, Jing Jin [1, 2], Qiucheng Wang [4]

1. Control Theory and Engineering, School of Astronautics, Harbin Institute of Technology, China
2. Shenzhen Engineering Lab for Medical Intelligent Wireless Ultrasonic Imaging Technology, Harbin Institute of Technology
3. 713rd Research Institute of central ship heavy industry, China
4. Department of Ultrasound, Harbin Medical University Cancer Hospital, China
E-mail: yue.zhao@hit.edu.cn, EstelleQi13@163.com, beauty@hit.edu.cn, jinjinghit@hit.edu.cn, 267355727@qq.com

***Abstract*—Minimally invasive surgery plays an important role in today's medical care. In the percutaneous insertion, the flexible needles have huge advantages. But due to the mechanical effect, the flexible needle will bend in the organs. So the advancing path must be planned before. In this paper, a path planning method based on a mechanical model is proposed. We improve the exploring algorithm and propose a cure path planning method using equal-radius arc which can avoid big return in the path. For practical need, we set the main obstacle as blood vessels. A blood vessel recognizing method is also proposed. Our path planning method concentrate on the following problems: 1) meet the physical characteristics of flexible needle; 2) reduce large return in the path; 3) reduce harm on the tissue. We choose the best path according to two indexes: rotating time and arc length. The simulation results of our blood vessel recognition and path planning method show that it can satisfy the practical demand.**

Keywords*—*flexible needles; needle insertion path planning; blood vessel recognizing method; minimally invasive surgery

I. INTRODUCTION

Minimally invasive surgery has become an inevitable trend for better surgical treatment thanks to the development of computer and medicine technology. As one of the most commonly used surgical technique, percutaneous insertion has been widely used in many kinds of surgical operations, such as living tissue pathological examination, local drug delivery, cancer therapy and so on [1][2]. During insertion, flexible needles have huge advantages over the traditional rigid needles. It is flexible and easy to achieve the curved trajectory, thus avoid obstacles like skeleton, nerve and blood vessel because of the deformation. It can also reach the target spot or area precisely, which is difficult for rigid needles.

To accomplish the puncture operation successfully, the needle insertion path planning is an essential step. This step is usually using the unicycle model [3], which is proposed by Webster to describe the motion of a bevel-tip flexible needle. Currently, the method of path planning mainly includes three types: numerical method, searching method and inverse solution. The numerical method includes the probability method and the objective function method. The numerical method optimizes the path by numerical calculation using the maximum or minimum value of the objective function. The probability method is first proposed by Alterovitz *et al.*[4].The best steering point has been calculated to reach the target with maximum probability. Besides, they also create the method of objective function [5]. In [4], on the basis of the finite element model of needle and tissue, the nonlinear objective function has been established to achieve the goal of shortest path, which satisfied the precision of the puncture, and can avoid the obstacles. The searching methods base on the characteristics of the path form, and use the artificial intelligence searching algorithms to search the feasible path. Xu *et al.* [6] conducted the Rapid-exploration Random Tree algorithm (RRT) to plan the flexible path of the needle in three-dimensional environment with obstacles. The inverse solution calculates the feasible path from the point of entry to the target using the inverse kinematics. Duindam *et al.* [7] proposed the use of inverse kinematics to calculate the spatial S 3D path.

However, the researches mentioned above are only appropriate for the off-line planning. The position and size of the obstacles are stochastic, not according with the actual situation. Moreover, the paths mostly have big returns, which do not meet the physical characteristics of flexible needles. To solve the first problem, we make full use of ultrasound images. In this paper, the puncture is supposed to perform in liver and the obstacles are mainly the liver vessels. First, the blood vessels are recognized in an ultrasound image and considered as the obstacles; then the insertion path is planned under consideration of the obstacles. In the planning, the method of arc interpolation is adopt to plan the curve path, which can accurately simulate the situation of the needle rotation in the tissue.

The remainder of the paper is organized as follows. In section II, the methods of blood vessel recognition and path planning based on the mechanical model are derived; in section III, the simulations and results are given; section IV gives the conclusion and the future work.

II. METHODS

A. Blood vessel recognition

Because of the different reflection coefficient of muscle, fat and blood of human, the blood vessels are darker than other tissue in an ultrasound image. We adopt a tube enhancement filter to recognize the blood vessels [7]. However, it is difficult to fix the scale σ of the Gaussian kernel due to the randomly appeared small low-echo area and the different sizes of the blood vessels. Therefore the multi-scale strategy is implemented to ensure the correct selection of the blood vessels. Since the speckle noise of US image is strong, if σ is close to the scale of one pixel, the noise could be strengthened. Actually, in the clinical US images, the radius of the cross section of vessels is no larger than 20 pixels, thus the largest scale $\sigma_{\max}$ should be set smaller than the largest size of the vessel, or the image could be over blurred. Since the main vessels in the liver are chosen, the smallest scale $\sigma_{\min}$ is larger than 5 pixels.

After confirming the range of the scale, the tube enhancement filter is used to extract the boundary of the vessel target [7]. The eigenvalue analysis of Hessian matrix can distinguish different geometrical structures, such as tube-like, plate-like and blob-like structures. The vessels appeared as a dark cylinder in the 3D US images, and the background is bright. According to [7] , the eigenvalues of the Hessian matrix λ_1、λ_2、λ_3 are used to present these features. For the area of blood vessels, the eigenvalues satisfy the conditions as:

$$|\lambda_1| \approx 0, |\lambda_1| << |\lambda_2|, \ \lambda_2 \approx \lambda_3 \tag{1}$$

For each pixel in the US image, its corresponding eigenvalues are calculated. To enhance the vessel region and filter out the background, a geometrical ratio which can distinguish the tube-like structure from the line-like and plate-like structure is calculated as [9]:

$$R_A = \frac{|\lambda_2|}{|\lambda_3|} \tag{2}$$

$$R_B = \frac{|\lambda_1|}{\sqrt{|\lambda_2 \lambda_3|}} \tag{3}$$

To distinguish the intensity differences between the target and background, a magnitude measurement parameter is calculated as:

$$S = \sqrt{\lambda_1^2 + \lambda_2^2 + \lambda_3^2} \tag{4}$$

Then, the tube enhancement measurement can be defined as:

$$v_0(\lambda) = \begin{cases} 0 & if\, \lambda_2 > 0\, or\, \lambda_3 > 0 \\ (1-\exp(-\frac{R_A^2}{2\alpha^2}))\exp(-\frac{R_B^2}{2\beta^2})(1-\exp(-\frac{S^2}{2c^2})) & \end{cases} \tag{5}$$

B. Path planning for the flexible needle

a. The mechanical model.

The path planning procedure is based on the following mechanical model. Here, we suppose that the needle could have deformation as ‘C’ because of the force from tissue during insertion

We mainly analyze the bending radius of the needle. The dashed line represents the cutting path of the needle, as shown in Fig. 1a. To simplify the model, the tissue is replaced by two loads $\delta_1(\xi)$、$\delta_2(\eta)$ of different directions. In Fig. 1, γ、β represent the cutting angles. When the tip of the needle contacts the tissue and moves forward, the tissue is split and generates force to resist the tip of the needle [10]. The forces $\omega_1(\xi)$, $\omega_2(\eta)$ are distributed along the bottom and the slope of the needle tipas shown in Fig. 1 b. The force and moments of force of the needle tip is shown in Fig. 1 c, here d represents the diameter of the needle and α represents the bevel angle of the needle tip. Thus, d and α can be used to express other variables in Fig. 1 c, which is shown as following:

$$\alpha = \gamma + \beta \tag{6}$$

$$a = d / \tan\alpha \tag{7}$$

$$b = d / \sin\alpha \tag{8}$$

$$e = d - a\tan\beta - b/3\sin\alpha \tag{9}$$

The forces $\omega_1(\xi)$、$\omega_2(\eta)$ distributed along the bottom and the slope meets the boundary condition which is expressed in the equations as below:

$$\omega_1(0) = K_T\delta_1(0) = K_T a\tan\beta \tag{10}$$

$$\omega_1(a) = 0 \tag{11}$$

$$\omega_2(0) = K_T\delta_2(0) = K_T b\tan\gamma \tag{12}$$

$$\omega_2(b) = 0 \tag{13}$$

here, K_T represents interaction stiffness between needle and tissue on unit length. Assuming that the load is distributed in a triangle, the concentrated force on the bevel and bottom of the needle can be calculated using equation (14) and (15).

$$F_1 = \int_0^a \omega_1(\xi)d\xi = \frac{K_T a^2}{2}\tan\beta \tag{14}$$

$$F_2 = \int_0^b \omega_1(\eta)d\eta = \frac{K_T b^2}{2}\tan\gamma \tag{15}$$

The joint force of the needle along the y direction at the tip of the needle is calculated in (16), and c is a constant.

$$Q = \frac{K_T a^2}{2}\tan\beta - \frac{K_T b^2}{2}\left(\frac{\tan\alpha - \tan\beta}{1+\tan\alpha\tan\beta}\right)(\cos\alpha - c\sin\alpha) \tag{16}$$

According to the approximate differential equation of the deflection curve in the cantilever beam, the curvature of any point of the flexible needle is obtained in equation (17) and (18). In this equation, l represents the length of the needle and Δl represents the distance from the needle to the fulcrum.

$$y' = \frac{d^2y}{d\Delta l^2} = \frac{M(\Delta l)}{EI} \tag{17}$$

$$M(\Delta l) = Q(l - \Delta l) \tag{18}$$

$$R = \frac{1}{y'} \tag{19}$$

b. Path planning

During the insertion, the flexible needle will bend because of the force interaction, which leads to the curve path. In the procedure of planning, a “stop-and-turn” strategy has been implemented [11]. In this strategy, the needle should stop moving forward at the spinning point and rotate a right angle. The planning can be divided into two parts: path node searching and curve path planning. Once the curve path is fixed in the previous step, the node searching step begins in the next step. Considering the actual situation, there should not be large returns on the insertion path. So the selection of searching nodes should be restricted to a certain angle. The whole process can be divided into six steps.

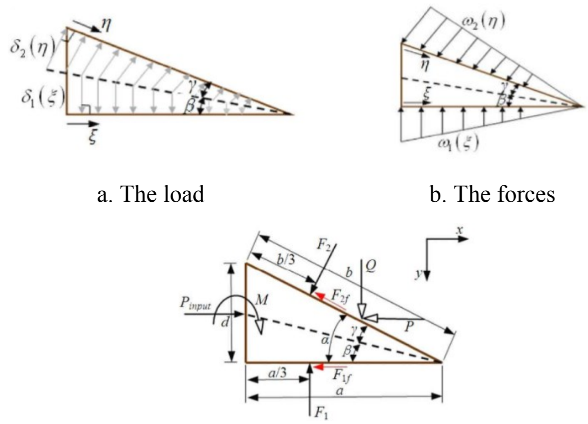

a. The load   b. The forces

c. The forces and moments of the needle tip

Fig.1 The demonstration of the mechanical model

- Step 1: First path node searching

First the whole space is discretized into a square grid, and the puncturing point is selected as the initial node. The lesion center is selected as the target node.Then a searching step begins to determine the nodes of these grids. Taking the initial node P_1 as the vertex, the connecting line between it and the target point P_t as the axis, a cone whose apex angle is $2\theta_1$, and height is the step length is drawn. The first node is selected within the plane of the bottom of the cone as shown in Fig. 2. The first planning plane is confirmed by a random point in space and the line connecting these two nodes.

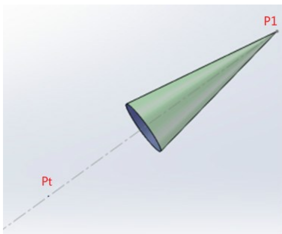

Fig.2 The selected range of the first node

- Step 2: Curve path planning in the first plane

The curve path is planned using equal-radius arc. We adopt the formula (17)-(19) to calculate the bending radius of the needle. There are two situations: if the chord length is enough for a whole arc with the calculated radius or not. If there are some sections of arc whose end are right on the straight line between the initial point and the first point, the center angles and the centers of these arcs are calculated directly according to the formula (20)、(21) and (22).

$$(x_2 - x_{01})^2 + (y_2 - y_{01})^2 = R^2 \tag{20}$$

$$(x_{01} - \frac{x_1 + x_2}{2})^2 + (y_{01} - \frac{y_1 + y_2}{2})^2 = R^2 - \frac{(x_2 - x_1)^2 + (y_2 - y_1)^2}{4} \tag{21}$$

$$\theta_{01} = 2arc\sin(\frac{\sqrt{(x_2 - x_1)^2 + (y_2 - y_1)^2}}{2R}) \tag{22}$$

here (x_1, y_1) 、 (x_2, y_2) represents node coordinates, (x_{01}, y_{01}) represents center coordinates and θ_{01} represents center angle. If the length of chord is not long enough for a whole arc, the curve paths in the first plane are solved using arc interpolation, as shown in Fig 3.Two equal-radius arcs are chosen to complete the following paths.

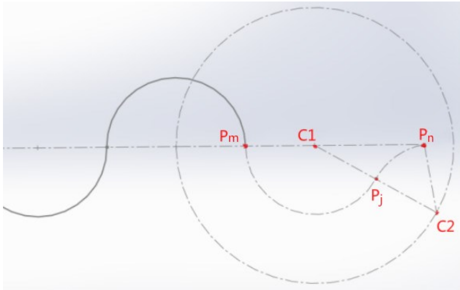

Fig.3 Arc interpolation

The demonstration of path planning on the first straight line is shown in Fig 4.

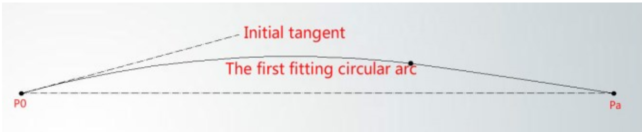

Fig.4 The demonstration of path planning

- Step 3: Judging of the whole curve path

Whether the path has reached the target point or not is judged. If so, the path planning is over; if not, it continues to step 4.

- Step 4:Next path planning

a: Next path node searching

First confirm the selection range of the end point in the second straight line. Taking the tangent vector of the arc at the end point of the first straight line as the axis, a cone is drawn the same way as Step 1. The end point selection range is also within the bottom of the cone, as shown in Fig 5. And the next path node P_a can be found.

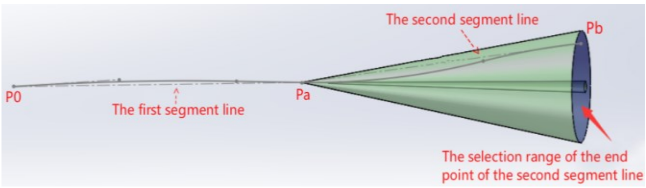

Fig.5 The selected range

b: Plane transition

First, the deflecting angle to the next plane is calculated according to the formula (23) - (25).

$$\vec{n}_2 = b \times l_2 \tag{23}$$

$$\theta_{p1} = \arccos(\vec{n}_1 \cdot \vec{n}_2) \tag{24}$$

$$\theta_{c1} = \arccos(\vec{l}_2 \bullet \vec{b}) \tag{25}$$

Here, the symbol $\vec{b}$ represents the tangent vector of the previous arc of the first straight line; $\vec{l}_2$ represents the unit vector of second straight line; $\vec{n}_1$ is the normal vector of the first plane, and $\vec{n}_2$ is the normal vector of second plane; θ_{p1}

represents the deflecting angle; θ_{c1} is the inserting angle of the first arc on the second plane.

c: Curve paths planning for the next planes

Once the followed plane is determined, Step 1 – Step 3 are repeated to plan the following curve paths in the corresponding plane.

d: Judging of the whole curve path

Just like the Step 3, if the path has reached the target point, the planning can be over; if not, continue to Step 4a to plan the path.

Moreover, the line connecting two nodes P_m and P_n may be close to or go through the blood vessel as Fig 6 shows. So the collision detecting module is essential. If there is a possibility of collision, this node will be given up.

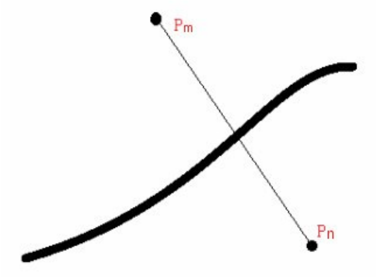

Fig.6 Collision

We can get different paths according to the method proposed above. Then the best path should be chosen. The evaluation parameters are set as the number of rotations of the whole path *N,* and the total length of the path *L*. We use the formula (26) to calculate the best path. The symbol w_1 and w_2 represent weight coefficients.

$$W = w_1 N + w_2 L \tag{26}$$

After the whole path is planned, the needle is punctured from the initial point in a constant speed with initial angle θ_0 . It moves forward and rotates according to the best planning path.

III. SIMULATIONS AND EXPERIMENTS

A. *Blood vessel simulation*

Several simulations using Field II [12][13] have been done. The parameters used are given in TABLE I.

TABLE I. PARAMETERS USED IN THE FIELD II SIMULATION

Name of parameter	Value
Transducer center frequency [MHz]	5
Sampling frequency [MHz]	100
Speed of sound [m/s]	1540
Wavelength	0.308
Width of element [mm]	0.154
Height of element [mm]	7
Kerf [mm]	0.0025
Focal position [mm]	(0,0,7)
Elements of the probe	64

A digital homogeneous phantom with three blood vessels whose radius is 9 mm is simulated. The middle lines of the three blood vessels are set as straight line, quadratic curve and cosine curve. The size of the phantom is 101*701*841 mm^3. For the homogeneous background, the spatial distribution of scatters is uniform distribution, and the spatial density of scatters is 100/mm^3. The reflection coefficient is Gauss distribution, with μ=0, σ^2=1. For the blood vessels, the spatial distribution of the scatters is uniform distribution with the spatial density of scatters 10/mm^3. The reflection coefficient is set as 0.1 for constant amplitude.

The ground truth position of the simulated blood vessel and the 2D cross sections of the simulated 3D ultrasound image is shown in Fig 7. The darker areas in Fig 7 a, b and c are the blood vessels.

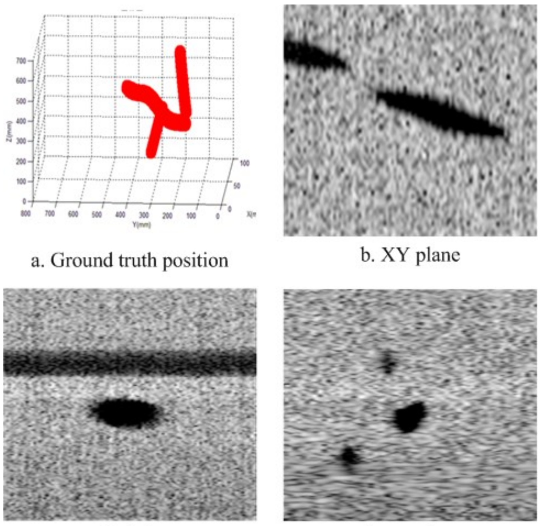

a. Ground truth position b. XY plane c. XZ plane d. YZ plane

Fig. 7 2D cross section of the simulated 3D ultrasound image and the real position of the vessels

B. *Real phantom*

Agar powder is used to make a practical body model sized 120*80*40 mm^3 as shown in fig 8.There are three tubes full of water standing for blood vessels in it. The ultrasound images of this phantom are obtained using the ultrasound equipment of Sonoscape with linear array. Since the three-dimensional probe can not be used in this experiment, so we adopt two-dimensional probe. To verify the blood vessel recognition in 3D situation, the 2D ultrasound images are put together to make a 3D ultrasound volume.

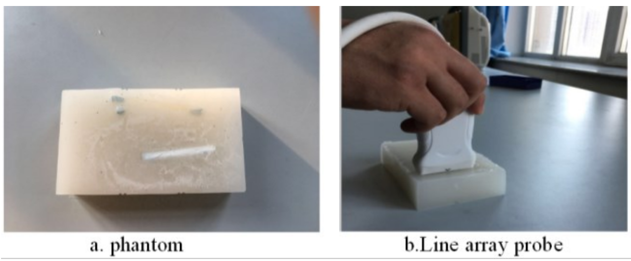

a. phantom b.Line array probe

Fig. 8 phantom and the experiment

a.The ultrasonic equipment b. Ultrasound image of the phantom

Fig. 9 the ultrasound equipment and the result

IV. Results

A. Blood vessel recognizing

After getting the 3D ultrasound image, a 3D medium filter of size 11 * 11 * 11 is used to preprocessing the image. The scale σ of the Gaussian kernel is set from 12 pixels to 20 pixels. And then the blood vessel is recognized by the multi-scale tube-like enhancement filter.

The three dimensional recognizing result is shown in Fig 10. It can be found that the recognizing result is relatively good comparing with the real position of the vessels in Fig 7a.

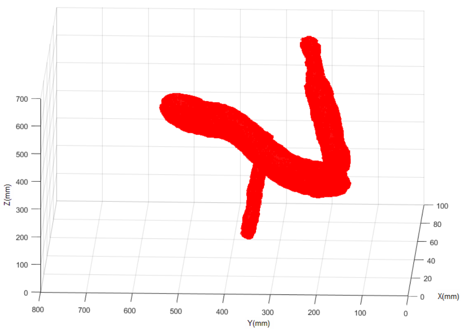

Fig. 10 3D recognizing result of the simulation volume

The 3D blood vessel recognition result of the real phantom is shown in Fig 11. Since the 3D ultrasound volume is made by 2D images, only one tube-like structure left in the volume. It was detected using the tube enhancement filter.

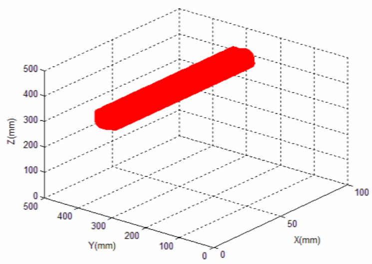

Fig. 11 The 3D recognizing result of the real phantom

B. Path planning

In the simulation of path planning procedure, a biopsy needle of 18 gauge (diameter 1.2 mm), 120 mm of length and 20 degree of dip angle is chosen to conduct the path planning. According to the mechanical model, the bending radius of the needle is set as 200mm. Moreover, the punturing angle and θ_1 are both 10 degrees and the step length is 74mm. The weight coefficients ω_1、 ω_2 are set as 0.7 and 0.3. We can get totally 12 paths which are different in rotation times and arc length according to the simulation result. To choose the best path, we use the formula (25) to compare different results and get the smallest one, which is shown in TABLE II. The best path is shown in Fig 12 and 13.

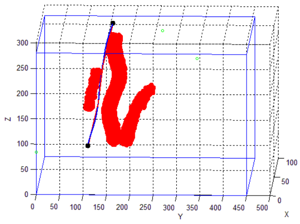

Fig. 12 The best path

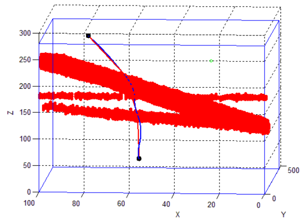

Fig. 13 The best path

From Fig 12 and 13, it can be seen that there is no collision and large returns on the planned path, the needle can get to the target point accurately. The rotating number is 5 and arc length is 234.19.

TABLE II. 12 Different Paths

Index of path	Arc length (mm)	Rotating times	W
1	234.70	5	73.91
2	234.73	5	73.92
3	234.44	5	73.83
4	234.38	5	73.81
5	234.24	6	74.47
6	234.16	6	74.45
7	234.30	5	73.79
8	**234.19**	**5**	**73.76**
9	234.16	6	74.45
10	234.28	5	73.79
11	234.28	5	73.78
12	234.43	5	73.83

V. Conclusions

In this paper, a strategy of the blood vessel recognizing and biopsy needle insertion path planning are combined together, which has a important meaning for minimally invasive surgery. The proposed blood vessel recognizing method is relatively accurate and can be used in real phantom. The planned path is made up of smooth connecting curves, which meets the requirement of the physical characteristics of puncture needles.

The future work will concentrate on the blood vessel recognizing method with more complex background. Moreover, a real time feedback in the path planning procedure should also be discussed and researched.

Acknowlendment

This study was partially funded by the National Natural Science Foundation of China (61501141), China Postdoctoral Science Foundation funded project (2016M590283) and the Postdoctoral Research Funds of

Heilongjiang Province (Grant No. LBH-Z15068). This work was also partially supported by Shenzhen Basic Research Program under grant JCYJ20160429115309834.

REFERENCES

[1] J Xiong, X Li, *et al*. Path Planning for Flexible Needle Insertion System Based on Improved Rapidly-exploring Random Tree Algorithm [C]. International Conference on Information and Automation, 2015.08

[2] Y Zhao, Y Shen *et al*., Evaluation and comparison of current biopsy needle localization and tracking methods using 3D ultrasound, Ultrasonics, 73: 206-220

[3] R. J. Webster III, N. J. Cowan, G. S. Chirikjian, *et al*. “Nonholmic Modeling of Needle Steering” [C] Proceedings of the 9th International Symposium on Experimental Robotics, Singapore, 2004: 35-44.

[4] R. Alterovitz, K. Goldberg, A. Okamura. “Planning for steerable bevel-tip needle insertion through 2D soft tissue with obstacles”, [C] Proceedings of the 2005 IEEE International Conference on Robotics and Automation, IEEE, 2005:1640-1645.

[5] R. Alterovitz, M. Branicky, K. Goldberg. “Motion planning under uncertainty for image-guided medical needle steering” [J] the International Journal of Robotics Research, 2008, 27(11-12): 1361-1374.

[6] Xu J, Duindam V, Alterovitz R, *et al*. Planning Fireworks Trajectories for Steerable Medical Needles to Reduce Patient Trauma [C]. Piscataway, NJ, USA: IEEE, 2009: 4517-4522.

[7] Duindam V, Xu J, Alterovitz R, et al.3D Motion Planning Algorithms for Steerable Needles Using Inverse Kinematics [C]. Heidelberg, D, Germany: Springer Verlag,2008:535-549.

[8] Frangi, A.F., *et al*., Multiscale vessel enhancement filtering, in Medical Image Computing and Computer-Assisted Interventation—MICCAI’98. 1998: p. 130-137.

[9] Moon, W.K., *et al*., Computer-aided tumor detection based on multi-scale blob detection algorithm in automated breast ultrasound
images. IEEE Transactions on Medical Imaging, 2013.

[10] Huimin Han. Study on friction and cutting model of oblique needle flexible puncture. [D] Harbin Institute of Technology.2012.07

[11] Jianjun Wang, Dong Sun, Jinjin Zheng and Wen Shang . “Optimal path planning for inserting a steerable needle into tissue.” International Conference on Information and Automation. Shenzhen, China.2011.6

[12] D. E. Robinson, F. Chen, and L. S. Wilson, “Measurement of velocity of propagation from ultrasonic pulse-echo data.”Ultrasound in medicine biology, vol. 8, no. 4, pp. 413-420, 1982.

[13] G. E. Trahey, J. W. Allison, and O. T. Von Ramm, “Angle independent ultrasonic detection of blood flow.”IEEE Transactions on Biomedical Engineering, vol. 34, no. 12, pp. 965-967, 1987